Advances in Materials Research, *Vol. 13, No. 4 (2024) 299-319*
https://doi.org/10.12989/amr.2024.13.4.299

Stochastic failure analysis of $[0/\theta]_s$ laminated composite plate containing edge crack and voids using XFEM

Ashok B. Magar*[1] and Achchhe Lal[2a]

[1]*Department of Mechanical Engineering, N.K.Orchid College of Engineering and Technology, Solapur 413002, India*
[2]*Department of Mechanical Engineering, S. V. National Institute of Technology, Surat 395007, India*

(*Received June 30, 2023, Revised February 8, 2024, Accepted February 13, 2024*)

Abstract. Due to higher strength-to-weight ratio of composite laminates, they find uses in many weight-sensitive applications like aerospace, automobile and marine structures. From a reliability point of view, accurate prediction of failure of these structures is important. Due to the complexities in the manufacturing processes of composite laminates, there is a variation in the material properties and geometric parameters. Hence stochastic aspects are important while designing the composite laminates. Many existing works of composite laminate failure analysis are based on the deterministic approach but it is important to consider the randomness in the material properties, geometry and loading to predict accurate failure loads. In this paper the statistics of the ultimate failure load of the $[0/\theta]_s$ laminated composite plate (LCP) containing the edge crack and voids subjected to the tensile loading are presented in terms of the mean and coefficient of variance (COV). The objective is to better the efficacy of laminate failure by predicting the statistics of the ultimate failure load of LCP with random material, geometric and loading parameters. The stochastic analysis is done by using the extended finite element method (XFEM) combined with the second-order perturbation technique (SOPT). The ultimate failure load of the LCP is obtained by ply-by-ply failure analysis using the ply discount method combined with the Tsai-Wu failure criterion. The aim is to know the effect of the stacking sequence, crack length, crack angle, location of voids and number of voids on the mean and corresponding COV of the ultimate failure load of LCP is investigated. The results of the ultimate failure load obtained by the present method are in good agreement with the existing experimental and numerical results. It is observed that $[0/\theta]_s$ LCPs are very sensitive to the randomness in the crack length, applied load, transverse tensile strength of the laminate and modulus of elasticity of the material, so precise control of these parameters is important. The novelty of the present study is, the stochastic implementation in XFEM for the failure prediction of LCPs containing crack and voids.

Keywords: coefficient of variance; crack; SOPT; stochastic; voids; XFEM

1. Introduction

Laminated composite plates (LCP) are commonly used in many structural engineering applications due to their advanced properties. Presence of the discontinuities like cracks and holes affects the stress distribution significantly. Parameter like fracture toughness is used to find the material resistance against the crack growth due to the applied loading. The stress intensity factor

*Corresponding author, Ph.D., E-mail: ashok.magar@gmail.com
[a]Ph.D., E-mail: achchhelal@med.svnit.ac.in

http://www.techno-press.org/?journal=amr&subpage=5 ISSN: 2234-0912 (Print), 2234-179X (Online)

(SIF) at the ultimate failure load of LCP is called fracture toughness. Evaluation of the ultimate failure load is required to get the fracture toughness of the LCP. The deterministic methods of getting the ultimate failure load of the LCP with discontinuities like cracks and voids are insufficient in the presence of uncertainties involved during manufacturing or in the physical characteristics of the plies. From the reliability point of view, the stochastic considerations are essential which accounts for these uncertainties.

The fracture analysis of LCPs containing discontinuities in the form of cracks, holes and inclusions is carried out by many researchers by using numerical methods like extended finite element method (XFEM) and extended isogeometric analysis (XIGA). In XFEM discontinuities and singularities can be modelled independent of the mesh. It is possible due to the notion of partition of unity (PUM) and level set method (LSM). Asadpoure and Mohammadi (2007) developed new enrichment functions for studying the fracture behavior of the orthotropic media containing cracks by using the extended finite element method (XFEM). The m-integral approach is used for stress calculation due to its higher accuracy. Asadpoure *et al.* (2006, 2006) used the method of partition of unity in the XFEM framework for fracture analysis of orthotropic media contacting cracks. The m-integral approach is used for calculating the stress intensity factors (SIF). Chen *et al.* (2019) presented a framework of adaptive extended isogeometric analysis (XIGA) for the fracture simulation of orthotropic composites containing discontinuities. The multiple-level set functions are used to capture the interfaces of the discontinuities. Jiang *et al.* (2014) developed the XFEM framework to evaluate the dynamic SIF of plates having more than one discontinuity. Dynamic SIF of major crack is significantly affected by the other discontinuities. Shedbale *et al.* (2013) studied the nonlinear fracture behavior of the plate containing discontinuities by using XFEM. SIFs are evaluated by using the J-integral method. The results are presented for the effect of discontinuities on the fatigue life of cracked plates. Natarajan *et al.* (2014) presented the fracture problem of crack-inclusion interactions in elastic media by using the XFEM. The crack tip SIFs are obtained by using the interaction integral method. Gu *et al.* (2020) developed the XIGA method using LR B splines for capturing the crack growth accurately through orthotropic as well as isotropic media. XIGA with local adaptive refinement is more accurate as well as converges faster. Nguyen *et al.* (2019) studied crack growth in the orthotropic media by using the extended nodal gradient FEM with thermo mechanical considerations. The singularity of displacements, temperature and heat flux in the presence of crack are defined by enrichment functions. Patil *et al.* (2017) used the XFEM along with the multi-scale FEM to model the matrix containing particles and/or voids. Through the simulations, properties of heterogeneous matrix are evaluated in less computational time. Sukumar *et al.* (2001) used the XFEM coupled with the level set method to locate the holes and material interfaces. The local enrichment at the material interface is obtained by using level set functions. Yu and Bui (2018) obtained high-performance and accurate solution for domains with discontinuities like multiple cracks and inclusions, and material interfaces by using a novel method based on XFEM. Kim and Paulio (2002) devolved a novel method based on the FEM to address the fracture behavior of orthotropic functionally graded materials (FGMs) with arbitrary crack orientations. SIFs are calculated by using the modified crack closure (MCC) and the displacement correlation technique (DCT) methods. Ebrahimi *et al.* (2008) did the fracture analysis of orthotropic media containing crack by using the XFEM combined with the partition of unity framework. The interaction integral method is used for the evaluation of J-integral. Bayesteh and Mohammadi (2013) investigated crack propagation in the orthotropic FGM media by using the XFEM. Bhardwaj *et al.* (2015) obtained the fatigue life of the FGM plate having an interfacial edge crack by using XIGA. The plate also contains other defects like minor cracks, holes and inclusion. The system input parameters for stochastic

analysis are generated by using the log-normal distribution. The effect of the randomness in the input parameters on the fatigue life of the FGM plate is presented in detail. Singh *et al.* (2012) used XFEM to get the solution of the fatigue life of isotropic plates having different discontinuities. Fatigue life is estimated by using the Paris fatigue law. Amongst all discontinuities, the effect of holes on fatigue life is very significant. Lei *et al.* (2005) evaluated the dynamic SIF in a cracked plate containing inclusions by using the boundary element method (BEM). For crack growth modeling; new elements having constant length are added at the crack tip. The behavior of moving crack in the presence of inclusions is presented. Wang and Hasebe (2000) presented the bending solution of the infinite plate containing a line crack and rigid inclusions. The stress functions are obtained by using a rational mapping function. Sharma *et al.* (2013) studied the effect of domain in-homogeneities on the SIF of the cracked plates using XFEM. The enrichment function is obtained by using the partition of unity method and discontinuity boundaries are traced by using level set method. Qin and Lu (2000) obtained stress and electric displacement (SED) intensity factors in thermo-piezoelectric solid containing interaction of multiple cracks and inclusions by using BEM. The results of SED for finite and infinite plate are accurate and match with other numerical results.

Liu *et al.* (2021) presented a new method based on the XFEM combined with the LaRC failure criteria for the damage analysis of LCP containing circular openings subjected to tensile loading. Intra-laminar failure is obtained by using LaRC failure criteria and the crack propagation and property degradation by using the XFEM. Kaman (2011) obtained the fracture toughness of the LCP with an edge crack and subjected it to tensile loading. Failure loads are obtained by the experiments and used to get the fracture toughness of LCP. Numerical investigation is done by using the ANSYS software. Critical SIFs are calculated by using the DCM Method. Benzaama *et al.* (2017) analyzed the fracture behavior of notched composite plates subjected to tensile loading. Failure load is obtained by using XFEM incorporated in ABAQUS software. Ezzine *et al.* (2018) studied the damage of riveted, bonded and hybrid joints in steel assemblies experimentally and numerically with XFEM. Patel *et al.* (2022) studied the fracture behavior and delamination of SiC ceramic matrix composites by using XFEM damage criteria combined with the cohesive zone modeling (CZM) method. Swati *et al.* (2018) presented the delamination of fibre-reinforced composites containing single and multiple cracks using ABAQUS with cohesive elements. Hulton and Cavallaro (2016) presented a comparative study of failure of FRP composites, numerically by XFEM and by experiments with lateral compression. Higuchi *et al.* (2016) used coupled XFEM/CZM modeling to get a progressive failure analysis of CFRP laminates. Abdullah *et al.* (2017) presented crack modeling and delamination of carbon-reinforced composites by using the XFEM tool of ABAQUS. Delamination prediction of composite is based on the maximum principal stress criteria. Dongen *et al.* (2018) modeled cracks in the matrix by using XFEM and delaminations by using the CZM method incorporated in the ABAQUS. Ma *et al.* (2021) proposed a new conforming augmented FEM formulation for predicting the inter ply failure. The new method is used to model the progressive failure of composites containing open holes. Duarte *et al.* (2021) presented a comparison of the failure of FRP composites containing circular hole by using XFEM and Hashin failure criteria. The effect of parameters like laminate stacking sequence, hole radius etc. on laminate failure behavior is presented.

The researchers have used the Monte Carlo Simulation (MCS) method for studying the fracture behavior of LCP with stochastic considerations. Martinez *et al.* (2021) developed a new stochastic machine-learning algorithm for the analysis of fracture problems with uncertainties in the framework of XFEM. Accuracy is high with very few training samples and coarse mesh. Lua *et al.* (1993) studied the crack growth under fatigue loading in the presence of uncertainties in the different input

parameters by using the probabilistic BEM. The stochastic results of the present method are compared with the results of the MCS method. Shen *et al.* (2021) developed a stochastic framework by using MCS and scaled boundary FEM for fracture problems. The results are presented for the uncertainty in the crack angle in an isotropic and bi-material plates. Khasin (2014) proposed a stochastic crack growth model based on Brownian motion. The methodology is applicable for different types of loading including the fatigue type loading. Hamdia *et al.* (2017) studied the stochastic fracture behavior of nano-composites by using a 2D FEM combined with phantom mode method for crack growth analysis. The polynomial chaos (PC) method is developed for the sensitivity analysis. Motamedi *et al.* (2014) presented a stochastic XFEM framework for the prediction of de-lamination in PPS or glass LCP in fracture mode I. The results are validated with the experimental data using the DCB tests. Palekar and Lal (2021) presented the stochastic behavior in terms of mean and COV of mixed mode SIF of symmetric LCP subjected to biaxial in-plane loading and containing a central crack. The formulation is based on the XFEM incorporated within the framework of SOPT. Nadjafi and Gholami (2021) presented the reliability studies of a LCP containing a circular hole subjected to tensile loading. Reliability analysis is done by using the first and second-order reliability method.

1.1 Gaps in the existing work

From the literature review presented in the introduction section, the following existing knowledge gaps have been identified,

- Many researchers have used numerical methods like the XFEM and XIGA extensively to deal with the singularity problems for studying the fracture behavior of the isotropic or FGM plates containing discontinuities by using a deterministic or stochastic approach.
- Few researchers have studied the deterministic fracture behavior of laminated composite plates (LCP) but uncertainty or stochastic aspects are not addressed.
- Deterministic failure analyses of composite laminated plates containing cracks have been studied by afew researchers experimentally and numerically by using XFEM combined with the CZM method. For the accurate prediction of the laminate failure loads, variations in the input parameters like material properties, geometry and loading of the laminate need to be considered. Considerations of uncertainties in the input parameters are not addressed in the existing work of failure analysis of composite laminated plates containing cracks.
- Voids are present in the composite laminates owing to the defects during the fabrication of laminates. In the presence of cracks and voids, failure loads are significantly reduced. In the available existing works on failure analysis of cracked plates, a consideration of voids in the analysis is missing.

1.2 Outline of the present work

To the best of the author's knowledge, the problem of getting the ultimate failure load of LCP containing edge crack and voids with stochastic considerations in material properties, geometric parameters and loading is not addressed. An ultimate failure load is required to get the fracture toughness of the cracked plates.

In the present work, the numerical study of the statistics of the mean and corresponding COV of ultimate failure load of $[0/\theta]_s$ LCP using the stochastic extended finite element method (SXFEM) is presented. The second-order perturbation technique (SOPT) method is used to obtain the mean and

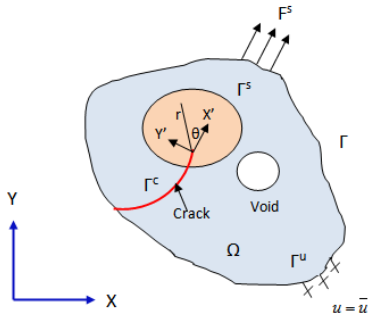

Fig. 1 Arbitrary orthotropic body in equilibrium

corresponding COV of the ultimate failure load of $[0/\theta]_s$ LCP. The Efficacy of the SOPT method is verified by comparing the SOPT results with the results obtained by using Monte Carlo simulation (MCS) and polynomial chaos (PC) methods.

The effect of different parameters like crack length, number of voids, location of the voids and crack angle on the mean and corresponding COV of ultimate failure load of $[0/\theta]_s$ LCP is presented in this paper. The individual and combined randomness are considered in the different input parameters associated with the material properties, geometry of the LCP and loading. The deterministic results of ultimate or critical failure load and critical SIF obtained by the present method are compared with the experimental results and they are in good agreement with the Kaman (2011).

2. Mathematical formulation

In this work, the general XFEM formulation of LCP presented by Mohammadi (2008) is used. An arbitrarily shaped orthotropic body containing crack and void is defined in global Cartesian coordinates (X, Y) and the axes of elastic symmetry are aligned with the local Cartesian coordinates axes ($x'y'$) defined on the crack tip as shown in Fig. 1. The Ω denotes the domain containing crack and void and Γ is the boundary of Ω. F^s and $\overline{u}$ are the external traction and prescribed displacement on Γ^s and Γ^u respectively. Crack and the void boundaries are traction free. In polar coordinate, $(\rho\theta)$ is defined locally at the crack tip.

2.1 XFEM formulation

The elastostatic equilibrium equations and respective boundary conditions for an orthotropic body in Fig. 1 can be written as Mohammadi (2008)

$$\nabla\sigma + F^b = 0 \text{in}\Omega \tag{1}$$

Boundary Conditions are

$$\begin{aligned} \sigma n &= F^s \text{on}\Gamma^s \\ u &= \overline{u}\ \text{on}\Gamma^u \\ \sigma n &= 0 \text{on}\Gamma^c \end{aligned} \tag{2}$$

Where F^b, F^s and $\overline{u}$ are body force, surface traction and prescribed displacement on Γ and n is a normal to the boundary Γ.

Consider a point 'x' in a two-dimensional space of the FE model with N representing a set of nodes. The approximate displacement of point 'x' is given by

$$u^h(x) = \overbrace{\sum_{K\in N} N_k(x)u_k}^{\text{ClassicalFEM}} + \overbrace{\sum_{l\in N_g} N_l(x)\Psi(x)a_l}^{\text{EnrichedFEM}} \tag{3}$$

Where, u_k represents the degrees of freedom (DOF) in classical FEM, $N_k(x)$ and $N_k(x)$ are shape functions associated with normal nodes and enriched nodes respectively. a_l are additional DOFs of nodes associated with discontinuity. $\Psi(x)$ is enrichment functions associated with discontinuity like crack, void or inclusions.

For LCP with edge crack and voids Eq. (3) becomes

$$\begin{aligned} u^h(x) = \sum_{k=1}^{n} N_k(x)u_k + \underbrace{\sum_{l=1}^{cr} N_l(x)\left(H\big(\zeta(x)\big) - H\big(\zeta(x_l)\big)\right)a_l}_{\text{Enrichmentofnodesoncrack face}} + \\ \underbrace{\sum_{s=1}^{tp1} N_s(x)\sum_{t=1}^{tpf}\big(F_t^1(x) - F_t^1(x_s)\big)b_s^1}_{\text{Enrichmentofnodesoncracktip1}} \\ + \underbrace{\sum_{s=1}^{tp2} N_s(x)\sum_{t=1}^{tpf}\Big(F_t^2(x) - F_t^2(x_s)\Big)b_s^2}_{\text{Enrichmentofnodesoncracktip2}} + \underbrace{\sum_{q=1}^{m} N_q(x)\left(\psi(x) - \psi\big(x_q\big)\right)v_q}_{\text{Emrichmentofnodesonvoids}} \end{aligned} \tag{4}$$

Where, 'cr', 'tp' and 'm' are the number of nodes on the crack face, crack tip and void respectively. 'a_l', 'b_s' and 'v_q' are additional DOF of the nodes of crack face, crack tip and voids respectively. $H\big(\zeta(x)\big)$ is a Heaviside function, defined on the positive side of the crack and otherwise

$$H\big(\zeta(x)\big) = \begin{cases} +1\zeta \in \Omega^+ \\ -1\zeta \in \Omega^- \end{cases} \tag{5}$$

$\psi(x)$ are Heaviside function associated with the enrichment of 'm' nodes of voids. $\psi(x)$ takes the value of +1 outside the void and 0 within the void.

$Fp(x)$ are the crack tip enrichment functions given by Mohammadi (2008) and defined in a polar coordinate system

$$\big(F_t(r,\theta)\big)_{t=1}^{4} = \left[\sqrt{r}\,cos\frac{\theta_1}{2}\sqrt{g_1(\theta)}, \sqrt{r}\,cos\frac{\theta_2}{2}\sqrt{g_2(\theta)}, \sqrt{r}\,sin\frac{\theta_1}{2}\sqrt{g_1(\theta)}, \sqrt{r}\,sin\frac{\theta_2}{2}\sqrt{g_2(\theta)}\right] \tag{6}$$

The global linear discrete XFEM equations can be written as Mohammadi (2008)

$$[K]\{U\} = \{F\} \tag{7}$$

Where, [K] is the global stiffness matrix, $\{U\}$ is the vector of total degrees of freedom (classical FEM+X-FEM) and $\{F\}$ is the force vector. The global stiffness matrix and force vectors are obtained by assembly of element matrices. Element stiffness matrix and force vectors are defined by Shedbale *et al.* (2013)

$$\left[K_{pq}^{e}\right] = \begin{bmatrix} K_{pq}^{uu} & K_{pq}^{ua} & K_{pq}^{ub} & K_{pq}^{uv} \\ K_{pq}^{au} & K_{pq}^{aa} & K_{pq}^{ag} & K_{pq}^{av} \\ K_{pq}^{bu} & K_{pq}^{ba} & K_{pq}^{bb} & K_{pq}^{bv} \\ K_{pq}^{vu} & K_{pq}^{va} & K_{pq}^{vb} & K_{pq}^{vv} \end{bmatrix} \tag{8}$$

$$\{F_p^e\} = \{F_p^u \quad F_p^a \quad F_p^{b_{t1}} \quad F_p^{b_{t2}} \quad F_p^{b_{t3}} \quad F_p^{b_{t4}} \quad F_p^v\} \tag{9}$$

$$\{U^e\} = \{u \quad a \quad b_{t1} \quad b_{t2} \quad b_{t3} \quad b_{t4} \quad v\} \tag{10}$$

Where

$$[K_{pq}^{rs}] = \int_{\Omega^e} (B_p^r)^T \, D B_q^s d\Omega (r,s = u,a,b,v) \tag{11}$$

$$f_p^u = \int_{\Gamma_s} N_p F^s d\Gamma + \int_{\Omega^e} N_p F^{b_t} d\Omega \tag{12}$$

$$f_p^a = \int_{\Gamma_s} N_p H F^s d\Gamma + \int_{\Omega^e} N_p H F^{b_t} d\Omega \tag{13}$$

$$f_p^{b_{t\kappa}} = \int_{\Gamma_s} N_p F_\kappa F^s d\Gamma + \int_{\Omega^e} N_p F_\kappa F^{b_t} d\Omega \, (\kappa = 1,2,3,4) \tag{14}$$

$$f_p^v = \int_{\Gamma_s} N_p (\psi(x) - \psi(x_i)) F^s d\Gamma + \int_{\Omega^e} N_p (\psi(x) - \psi(x_i)) F^{b_t} d\Omega \tag{15}$$

In Eq. (11) '*D*' is a material property matrix for LCP and '*B*' is a matrix of derivatives of shape functions. '*D*' for LCP is evaluated using the procedure of Jones (2002)

$$D_{lm} = \sum_{n=1}^{NL} \int_{z_{n-1}}^{z_n} \overline{Q_{lm}}(1,z) \, dz \, (l,m = 1,2,6) \tag{16}$$

Where, *NL* represents a number of layers in LCP, $\overline{Q}_{lm}$ represents reduced transformed stiffness terms and 'z' is coordinate in the thickness direction.

[*B*], matrix of derivatives of shape functions is given by

$$B_p^u = \begin{bmatrix} N_{p,x'} & 0 \\ 0 & N_{p,y'} \\ N_{p,y'} & N_{p,x'} \end{bmatrix} B_p^a = \begin{bmatrix} (N_p H)_{,x'} & 0 \\ 0 & (N_p H)_{,y'} \\ (N_p H)_{,y'} & (N_p H)_{,x'} \end{bmatrix} \tag{17}$$

$$B_p^{b_{tk}} = \begin{bmatrix} (N_p F_k)_{,x'} & 0 \\ 0 & (N_p F_k)_{,y'} \\ (N_p F_k)_{,y'} & (N_p F_k)_{,x'} \end{bmatrix} (k = 1,2,3,4) \tag{18}$$

$$[B_p^{b_t}] = [B_p^{b_{t1}} \quad B_p^{b_{t2}} \quad B_p^{b_{t3}} \quad B_p^{b_{t4}}] \tag{19}$$

$$B_p^v = \begin{bmatrix} \left(N_p \left(\psi(x) - \psi(x_p)\right)\right)_{,x'} & 0 \\ 0 & \left(N_p \left(\psi(x) - \psi(x_p)\right)\right)_{,y'} \\ \left(N_p \left(\psi(x) - \psi(x_p)\right)\right)_{,y'} & \left(N_p \left(\psi(x) - \psi(x_p)\right)\right)_{,x'} \end{bmatrix} \tag{20}$$

2.2 Stress intensity factor(SIF) evaluation

In the present study, to evaluate the mixed mode SIFs KI and KII of the LCP, the domain integral method of Mohammadi (2008) is used.

$$J = \int_A \left(\sigma_{ij}\frac{\partial u_j}{\partial x} - W_{st}\Delta_{1j}\right)\frac{\partial q}{\partial x_j}dA \tag{21}$$

Where, A is the domain around the crack tip as shown in Fig. 1. Δ_{1j} is a Kronecker delta, W_{st} represents the strain energy density and 'q' is a function having value one at the crack tip and zero at the boundary Γ. For a given geometry, two equilibrium states correspond to the actual state and an auxiliary state. The auxiliary stress and displacement fields are written as

$$\begin{aligned}\sigma_{11}^{aux} = {} & \frac{K_I^{aux}}{\sqrt{2\pi r}} Re\left[\frac{s_1 s_2}{s_1 - s_2}\left\{\frac{s_2}{\sqrt{\cos\theta + s_2\sin\theta}} - \frac{s_1}{\sqrt{\cos\theta + s_1\sin\theta}}\right\}\right] \\ & + \frac{K_{II}^{aux}}{\sqrt{2\pi r}} Re\left[\frac{1}{s_1 - s_2}\left\{\frac{s_2^2}{\sqrt{\cos\theta + s_2\sin\theta}} - \frac{s_1^2}{\sqrt{\cos\theta + s_1\sin\theta}}\right\}\right]\end{aligned} \tag{22}$$

$$\begin{aligned}\sigma_{22}^{aux} = {} & \frac{K_I^{aux}}{\sqrt{2\pi r}} Re\left[\frac{1}{s_1 - s_2}\left\{\frac{s_1}{\sqrt{\cos\theta + s_2\sin\theta}} - \frac{s_2}{\sqrt{\cos\theta + s_1\sin\theta}}\right\}\right] \\ & + \frac{K_{II}^{aux}}{\sqrt{2\pi r}} Re\left[\frac{1}{s_1 - s_2}\left\{\frac{1}{\sqrt{\cos\theta + s_2\sin\theta}} - \frac{1}{\sqrt{\cos\theta + s_1\sin\theta}}\right\}\right]\end{aligned} \tag{23}$$

$$\begin{aligned}\sigma_{12}^{aux} = {} & \frac{K_I^{aux}}{\sqrt{2\pi r}} Re\left[\frac{s_1 s_2}{s_1 - s_2}\left\{\frac{1}{\sqrt{\cos\theta + s_1\sin\theta}} - \frac{1}{\sqrt{\cos\theta + s_2\sin\theta}}\right\}\right] \\ & + \frac{K_{II}^{aux}}{\sqrt{2\pi r}} Re\left[\frac{1}{s_1 - s_2}\left\{\frac{s_1}{\sqrt{\cos\theta + s_1\sin\theta}} - \frac{s_2}{\sqrt{\cos\theta + s_2\sin\theta}}\right\}\right]\end{aligned} \tag{24}$$

And

$$\begin{aligned}u_1^{aux} = {} & K_I^{aux}\sqrt{\frac{2r}{\pi}} Re\left[\frac{1}{s_1 - s_2}\left\{s_1 p_2\sqrt{\cos\theta + s_2\sin\theta} - s_2 p_1\sqrt{\cos\theta + s_1\sin\theta}\right\}\right] \\ & + K_{II}^{aux}\sqrt{\frac{2r}{\pi}} Re\left[\frac{1}{s_1 - s_2}\left\{p_2\sqrt{\cos\theta + s_2\sin\theta} - p_1\sqrt{\cos\theta + s_1\sin\theta}\right\}\right]\end{aligned} \tag{25}$$

$$\begin{aligned}u_2^{aux} = {} & K_I^{aux}\sqrt{\frac{2r}{\pi}} Re\left[\frac{1}{s_1 - s_2}\left\{s_1 q_2\sqrt{\cos\theta + s_2\sin\theta} - s_2 q_1\sqrt{\cos\theta + s_1\sin\theta}\right\}\right] \\ & + K_{II}^{aux}\sqrt{\frac{2r}{\pi}} Re\left[\frac{1}{s_1 - s_2}\left\{q_2\sqrt{\cos\theta + s_2\sin\theta} - q_1\sqrt{\cos\theta + s_1\sin\theta}\right\}\right]\end{aligned} \tag{26}$$

Where, s_1 and s_2 are the roots of the characteristic equation (Eq. (27)) obtained by using compatibility and equilibrium equation

$$C_{11}S^4 - 2C_{16}S^3 + (2C_{12} + C_{66})S^2 - 2C_{26}S + 2C_{22} = 0 \tag{27}$$

Coefficients of 'S' in Eq. (27) are the compliance coefficients. p_1, p_2, q_1 and q_2 in Eq. (25)-(26) are defined as

$$p_i = C_{11}S_i^2 + C_{12} - C_{16}S_i \text{ and } q_i = C_{12}S_i + \frac{C_{22}}{S_i} - C_{26}\, i = 1,2 \tag{28}$$

The 'J' integral is obtained by superposition as

$$J = J^{act} + J^{aux} + M \tag{29}$$

Where, J^{act} and J^{aux} are corresponding to actual and auxiliary state and M integral is given as

$$M = \int_A \left(\sigma_{ij} \frac{\partial u_i^{aux}}{\partial x} + \sigma_{ij}^{aux} \frac{\partial u}{\partial x} - W_{st} \Delta_{1j}\right) \frac{\partial q}{\partial x_j} dA \tag{30}$$

For linear elasticity

$$W_{st}^m = \frac{1}{2}\left(\sigma_{ij}\varepsilon_{ij}^{aux} + \sigma_{ij}^{aux}\varepsilon_{ij}\right) \tag{31}$$

The evaluation of Eq. (31) gives

$$M = 2P_{11}K_I K_I^{aux} + P_{12}(K_I K_{II}^{aux} + K_I^{aux} K_{II}) + 2P_{22}K_{II}K_{II}^{aux} \tag{32}$$

Where

$$P_{11} = -\frac{C_{22}}{2} Im\left(\frac{S_1+S_2}{S_1 S_2}\right), P_{12} = -\frac{C_{22}}{2} Im\left(\frac{1}{S_1 S_2}\right) + \frac{C_{11}}{2} Im(S_1 S_2), P_{12} = \frac{C_{11}}{2} Im(S_1 + S_2) \tag{33}$$

Simultaneous equations are obtained as below by using two states $[M^1(K_I^{aux} = 1, K_{II}^{aux} = 0)$ and $M^2(K_I^{aux} = 0, K_{II}^{aux} = 1)]$ in Eq. (32).

$$M^1 = 2P_{11}K_I + P_{12}, M^2 = P_{12}K_I + 2P_{22}K_I \tag{34}$$

By solving simultaneous Eq. (34), mixed mode SIFs are obtained.

2.3 Ultimate failure load of LCP with crack and void

By using the crack tip stresses ($\sigma_{ij}(i,j = 1,2,6)$) in the Tsai -Wu criteria, the first ply failure (FPF) load is obtained. The ultimate failure load of the LCP with edge crack and void is obtained by the progressive failure analysis (PFA). The ply discount method with the failure-based degradation in the material properties is used for the PFA.

The generalized equation for the Tsai-Wu theory is given as

$$F_j\sigma_j + F_{ji}\sigma_j\sigma_i \geq 1 \tag{35}$$

The coefficients Fji in the Eq. (35) are the functions of the material strength parameters and given as

$$F_1 = \frac{1}{X_T} - \frac{1}{X_C};\ F_2 = \frac{1}{Y_T} - \frac{1}{Y_C};\ F_{11} = \frac{1}{X_T X_C};\ F_{22} = \frac{1}{Y_T Y_C};\ F_{66} = \frac{1}{S^2};\ F_{12} = -\frac{1}{2}\sqrt{X_T X_C Y_T Y_C}$$

Where, X_T and X_C are the longitudinal tensile and compressive strength respectively, Y_T and Y_C are transverse tensile and compressive strength respectively and S is the shear strength.

The initial step in the PFA is to evaluate the first ply failure load (FPFL) by using the Tsai-Wu criteria. After getting the FPFL, the failed ply property degradation is based on the H_i index as per Singh and Kumar (1998). H_i indexes are the failure mode dependent. Once the H_i index of the failed ply is calculated, the material properties are degraded corresponding to the index having maximum value amongst the all the H_i indexes. $H_1 = F_1\sigma_1 + F_{11}\sigma_1^2$ defines the fiber failure, if H_1 is the largest amongst all the H_i index then E_1 is degraded. Similarly, corresponding to $H_2 = F_2\sigma_2 + F_{22}\sigma_2^2$, E_2 is degraded and $H_6 = F_{66}\sigma_6^2$ corresponds to degradation of G_{12}. The degradation in the

properties of the failed ply causes the redistribution of the stresses at the crack tip. The new stress field at the crack tip is obtained after degradation in the material properties and the failure of the new ply is ascertained. This process is repeated till the last ply failure (LPF) occurs. The load corresponding to the LPF is the ultimate failure load of the LCP.

2.4 Second order purturbation technique (SOPT)

In the present study, the stochastic response of $[0/\theta]_s$ LCP is expressed in terms of the mean and coefficient of variance (COV) of ultimate failure load. The randomness is considered in the different system input parameters. The second-order perturbation technique (SOPT) based on the Taylor series of expansion is used in the present stochastic analysis. The main advantage of this method is less computational time.

In the SOPT method second order variance is not available hence first order variance is considered along with the second order mean as Haldar and Mahadevan (2000). The ultimate failure load (F_L) is considered as a function of random variables b_i (i=1, 2…, 11) with mean μ_{b_i} and standard deviation σ_{b_i}. F_L by the Taylor series expansion is expressed as Haldar and Mahadevan (2000)

$$F_L = F_L\left(\mu_{b_1},\ \mu_{b_2},\ldots,\ \mu_{b_i}\right) + \sum_{i=1}^{m}\left(b_i - \mu_{b_i}\right)\frac{\partial F_L}{\partial b_i} + \frac{1}{2}\sum_{i=1}^{m}\sum_{j=1}^{m}\left(b_i - \mu_{b_i}\right)\left(b_j - \mu_{b_j}\right)\frac{\partial^2 F_L}{\partial b_i\,\partial b_j} \quad (36)$$

The first-order mean of F_L is represented by $Q\left(F_L^{'}\right)$, which can be written as

$$Q\left(F_L^{'}\right) \approx F_L\left(\mu_{b_1},\ \mu_{b_2},\ldots,\ \mu_{b_i}\right) \quad (37)$$

The first-order variance of ultimate failure load (F_L) can be written as

$$\mathrm{var}(F_L) = \sum_i^r \sum_j^r \left[\left(\frac{\partial F_L}{\partial b_i}\right)\left(\frac{\partial F_L}{\partial b_j}\right)\right] cov\left(b_i, b_j\right) \quad (38)$$

$$\mathrm{cov}\left(b_i, b_j\right) = [C] \quad (39)$$

Where, $[C]$ is given by

$$[C] = \begin{bmatrix} \sigma_{b_1}^2 & cov(b_1,b_2) & \cdots & cov(b_1,b_i) \\ cov(b_1,b_2) & \sigma_{b_2}^2 & \cdots & cov(b_2,b_i) \\ \cdots & \cdots & \cdots & \cdots \\ cov(b_i,b_1) & cov(b_i,b_1) & \cdots & \sigma_{b_i}^2 \end{bmatrix} \quad (40)$$

Where, $\sigma_{b_1},\ \sigma_{b_2},\ \cdots,\ \sigma_{b_n}$ are

$$\sigma_{b_1}, \sigma_{b_2}, \ldots, \sigma_{b_i} = \mathrm{cov}(b_1, b_2, \ldots, b_i) x F_L\left(\mu_{b_1},\ \mu_{b_2},\ldots,\ \mu_{b_i}\right) \quad (41)$$

Where $\mathrm{cov}(b_1, b_2, \ldots, b_i)$ and $F_L\left(\mu_{b_1},\ \mu_{r_{b2}},\ldots,\ \mu_{b_i}\right)$ are COV of random input parameters and corresponding mean values respectively.

The second-order mean of the ultimate failure load (F_L) and corresponding variance is obtained by using SOPT (Haldar and Mahadevan 2000)

$$Q\left(F_L^{''}\right) = F_L\left(\mu_{b_i}\right) + \frac{1}{2}\mathrm{var}(F_L) \quad (42)$$

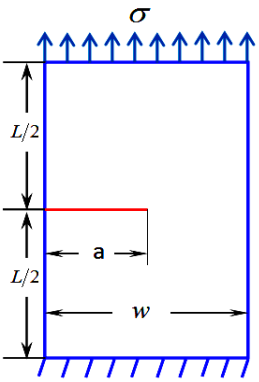

(a) Laminate-1 - LCP with edge crack

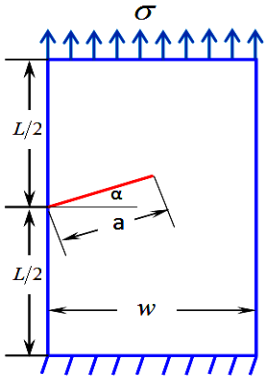

(b) Laminate-2 - LCP with inclined edge crack

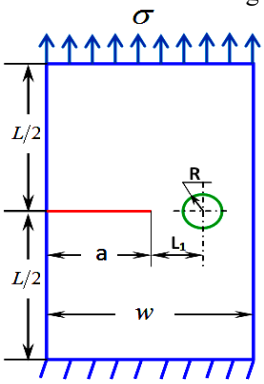

(c) Laminate-3 - LCP with edge crack and inline void

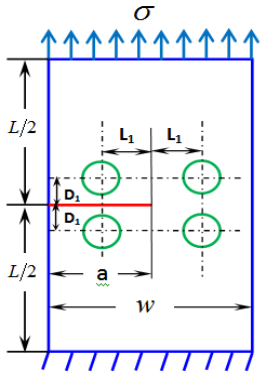

(d) Laminate-4 –LCP with edge crack and multiple voids

Fig. 2 Configurations of LCPs with edge crack and voids

$$\mathrm{var}\left(F_L^{''}\right) = \mathrm{var}(F_L) \tag{43}$$

After getting the variance of the response function, the standard deviation (SD) and COV of the response function (F_L) are obtained by dividing SD by the mean value of the F_L.

It is difficult to get the derivative of the response function with respect to the random input parameter (b_i) hence these derivatives are obtained by using the central difference method.

$$\frac{\partial F_L}{\partial b_i} = \frac{F_L(b_i+\delta b_i)-F_L(b_i-\delta b_i)}{2b_i\delta b_i} \tag{44}$$

The efficacy of the SOPT method is validated by comparing SOPT results with the results of Monte Carlo Simulation (MCS) and polynomial chaos (PC) methods.

3. Result and discussion

The configurations of the [0/θ]$_s$ LCP with edge crack and voids analyzed in the present study are shown in Fig. 2. The different values of θ used in the present study are 150, 300, 450, 600, 750 and 900. The dimensions of LCP considered in the present study are, length (L)=203.2 mm, width

Table 1 Properties of $[0/\theta]_s$ LCP along x and y axis

Stacking sequence $[0/\theta]_s$	E_x (MPa)	E_y (MPa)	G_{xy} (MPa)	v_{xy}
$[0/15]_s$	1.91×10^5	1.076×10^4	6.514×10^3	0.511
$[0/30]_s$	9.771×10^4	1.143×10^4	1.184×10^4	0.546
$[0/45]_s$	9.238×10^4	1.339×10^4	1.050×10^4	0.474
$[0/60]_s$	9.129×10^4	1.922×10^4	6.572×10^3	0.329
$[0/75]_s$	9.180×10^4	4.007×10^4	4.311×10^3	0.139
$[0/90]_s$	9.230×10^4	9.230×10^4	3.638×10^3	0.038

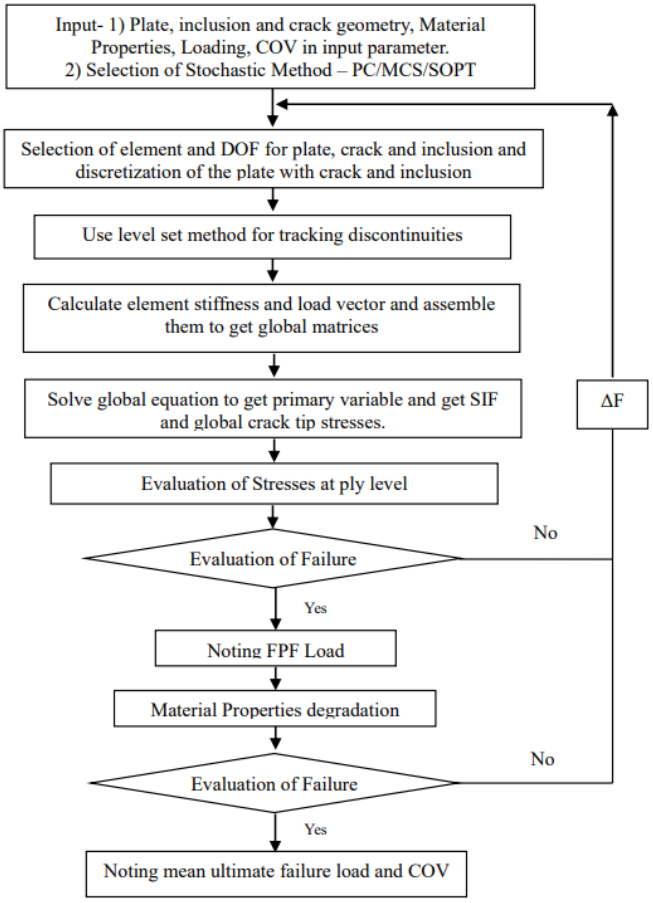

Fig. 3 Flow chart of proposed method

(w)=18 mm, thickness (t)=1.235 mm and crack length (a)=9 mm unless not specifically mentioned. The top edge of the LCP is subjected to uniform tensile loading and the bottom edge is clamped. R is the radius of the voids present in the LCP. In this analysis, the material properties of carbon epoxy $[0/\theta]_s$ LCP listed in Table 1 are used. These properties are taken from the Kaman (2011). The strength values of carbon epoxy laminate in tension, compression and shear are X_T=1441 MPa, Y_T=37MPa, X_C=420 MPa, Y_C=116 MPa and S=57 MPa taken from the Turan (2014).

Table 2 Results of convergence study

Number of elements	Ultimate failure load in 'N'	Percentage (%) error relative to 2500 element mesh
2500	4968.11	0
2116	4968.46	0.007
1936	4988.11	0.40
1296	5171.43	4.09
676	6011.04	20.99

Table 3 Validation of failure load and critical SIF

Stacking sequence $[0/\theta]_s$	Failure load (N)			Critical SIF (MPa$\sqrt{mm}$)	
	Present	Kaman (2011) Experimental	Error (%)	Present	Kaman (2011) Experimental
$[0/15]_s$	6442.3	6516.112	1.13276	4226.9	4404.62
$[0/30]_s$	4968.4	5145.807	3.4476	3142.2	3478.88
$[0/45]_s$	4665.7	4722.581	1.20445	2926.6	3192.76
$[0/60]_s$	5211.9	5229.024	0.32748	3470.4	3535.14
$[0/75]_s$	4265.1	4193.829	1.699426	2592.3	2835.29
$[0/90]_s$	3608.4	3680.767	1.96608	2377	2488.43

Fig. 3 shows a flow chart depicting the procedure of getting the mean and COV of the ultimate failure load (F_L) by using the proposed method.

For the probabilistic failure analysis of $[0/\theta]_s$ LCP, the second order perturbation technique (SOPT) method is used which is a non sampling method and requires a least computation time. For the stochastic analysis, the variation in the input random variables (RVs) is taken between 5 to 10% from the mean deterministic values of RVs. Eleven RVs representing randomness in geometric, material and loading parameters are considered in this study and they are represented by notation b_i [{i=1,2….11}] henceforth. The sequence of these RVs is as given below,

$b_1=E_1$, $b_2=E_2$, $b_3=G_{12}$, $b_4=\nu_{12}$, $b_5=X_T$, $b_6=Y_T$, $b_7=S$, $b_8=q$, $b_9=X_C$, $b_{10}=Y_C$, $b_{11}=a$. Where, E_1, E_2, G_{12} and ν_{12} are elastic modulus and Poisson's ratio, X_T, Y_T, X_C, Y_C and S are strength parameters in tension, compression and shear respectively. 'q' and 'a' are load and crack length respectively.

3.1 Validation study

In XFEM, the selection of the number of elements or mesh size is important to get accurate results, hence convergence study is required. The solution of the ultimate failure load of $[0/30]_s$ laminate-1 (Fig. 2(a)) is presented in Table 2 by considering the different mesh sizes. From Table 2, it is clear that the solution of the ultimate failure load is converging for 2116 elements; hence the numerical analysis in the present work is done by taking this number of elements.

Critical SIF obtained numerically by Kaman (2011) by using Ansys software and using PLANE82 element for $[0/60]_s$ laminate is 3501 MPa$\sqrt{mm}$ and by the present method is 3470.4 MPa$\sqrt{mm}$, which is close with the Ansys result.

Table 3 shows the validation results of the ultimate failure loads (F_L) and critical SIF of $[0/\theta]s$ LCP (laminate-1, Fig. 2(a)). The F_L and critical SIF obtained by the present method are in close

Table 4 Mean and corresponding COV of FL of LCP by using MCS, PC and SOPT methods

RV (b_i)	COC	Mean			COV		
		MCS	PC	SOPT	MCS	PC	SOPT
E_1	0.05	4968.7	4968.4	4968.4	0.010164	0.011513	0.0104
	0.1	4968.6	4968.2	4968.4	0.020922	0.020773	0.020815
E_2	0.05	4968.8	4968.2	4968.4	0.027877	0.02698	0.027452
	0.1	4969.4	4968.3	4968.4	0.055147	0.5561	0.055086
a	0.05	4968.5	4968.7	4968.4	0.1391	0.1376	0.134571
	0.1	4969.5	4968.6	4968.4	0.2492	0.2561	0.25277

Table 5 Effect of the randomness in the individual system parameter b_i (i=1-11) on the mean and corresponding COV of the F_L of $[0/30]_s$ LCP

i	RV (b_i)	COC	Mean	COV
1	E_1	0.05	4968.4	0.0104
		0.1	4968.4	0.020815
2	E_2	0.05	4968.4	0.027452
		0.1	4968.4	0.055086
3	G_{12}	0.05	4968.4	0.020507
		0.1	4968.4	0.041059
4	ν_{12}	0.05	4968.4	0.001266
		0.1	4968.4	0.002531
5	a	0.05	4968.4	0.134571
		0.1	4968.4	0.25277
6	X_T	0.05	4968.4	0.001084
		0.1	4968.4	0.001665
7	Y_T	0.05	4968.4	0.095003
		0.1	4968.4	0.18998
8	S_S	0.05	4968.4	0.010811
		0.1	4968.4	0.02186
9	q	0.05	4968.4	0.10025
		0.1	4968.4	0.20202
10	X_C	0.05	4968.4	0.005758
		0.1	4968.4	0.011607
11	Y_C	0.05	4968.4	0.000858
		0.1	4968.4	0.00172

agreement with the experimental values of F_L and critical SIF obtained by Kaman (2011). In the present solution, the maximum error occurring in the F_L is 3.45%. The F_L and the critical SIF magnitudes decrease as the angle θ in $[0/\theta]_s$ LCP changes from 15^0 to 90^0. If the applied load is along the fibre direction, the failure load is highest and as the angle between the applied load and

ply direction increases then failure load also decreases. It is because lamina strength is high in the fibre direction. The numerical solution of the ultimate failure load is useful for getting the fracture toughness of LCP.

3.2 The Stochastic analysis of [0/θ]s LCP

Table 4 shows the comparison of the results of the mean and corresponding COV of the ultimate failure load (F_L) of $[0/30]_s$ LCP (Laminate-1 Fig. 2(a)). The stochastic analysis is performed by using MCS, PC and SOPT methods by taking the random input system parameters as $b_i[\{i=1, 2, 5\}=0.05$ to 0.1]. As observed from Table 4, the results of the mean and corresponding COV of the ultimate failure load of LCP obtained by using the SOPT method closely agree with the results of the MCS and PC methods. This proves the efficacy of the SOPT method for the stochastic analysis of the LCP containing the edge crack and voids by using XFEM. As the MCS and PC methods are sampling-based hence require a large number of samples and more computational time.

The effect of the randomness in the individual RV $b_i[\{(i=1\text{-}11)\}=0.05$ to 0.1] on the mean and corresponding COV of the ultimate failure load (F_L) of $[0/30]_s$ LCP (Laminate-1, Fig. 2(a)) is presented in Table 5. Higher magnitudes of COV of ultimate failure load are observed corresponding to the input system parameters $b_i[i=1, 2, 3, 5, 7$ and 9] i.e., longitudinal, transverse, shear modulus of laminate, crack length, transverse strength of laminate and loading. These parameters need to be properly controlled to get the reliable response of the LCP containing edge crack. The material properties along with strength parameters of the laminates are governed by ply orientation and the variation in properties and strength is caused due to the inaccuracies in ply angles during the manufacturing of the laminates. As the Tsai-Wu failure criteria equation involves the crack tip stresses and terms related to strength parameters, they are highly sensitive to ultimate failure load. Variation in the crack length causes variation in stress concentrations at the crack tip and also affects the strength of the plate hence we get a higher value of COV corresponding to variation in the crack length.

To know the effect of the crack length on the mean and corresponding COV of F_L of $[0/\theta]_s$ LCP, laminate1 in Fig. 2(a) is chosen. In the present study, the crack length to plate width ratio a/w is varied from 0.2 to 0.6. Fig. 4 shows the variation of the mean of ultimate failure load (F_L) of $[0/\theta]_s$ LCP with respect to a/w ratio. F_L decreases as a/w ratio is increased because as the crack length increases, the magnitude of the crack tip stresses increases. F_L is maximum for the $[0/15]_s$ LCP plate and minimum for the $[0/90]_s$ LCP for all the crack lengths. F_L is a maximum for a lamina if the direction of the applied loading is closely aligned with the fibre orientation of the lamina. Because the lamina strength is higher along the fibre direction of the lamina i.e. along the longitudinal direction. In the case of the crack length, as the crack length increases the stress concentration at the crack tip intensifies as well as laminate weakens with an increase in the crack length. Hence with an increase in crack length, F_L decreases.

Fig. 5 shows the variation of COV of F_L of $[0/\theta]_s$ LCP due to a change in a/w ratio. The randomness is considered in the crack length 'a' with COC as 0.1. As seen from the Fig. 5 COV is very sensitive to crack length as well as laminate orientation. As seen from Table 5, a 5 to 10 % variation in crack length causes a deviation of COV of F_L by 13.46 to 25.28% hence F_L is very sensitive to variation in crack length. As the crack length increases i.e. a/w ratio increases, the COV of F_L increases due to higher stress concentrations at the crack tip and weakening of the plate.

To understand the effect of the inline void on the mean and corresponding COV of F_L of $[0/\theta]_s$ LCP, laminate-3 in Fig. 2(c) is chosen. The distance between the crack tip and the void centre is

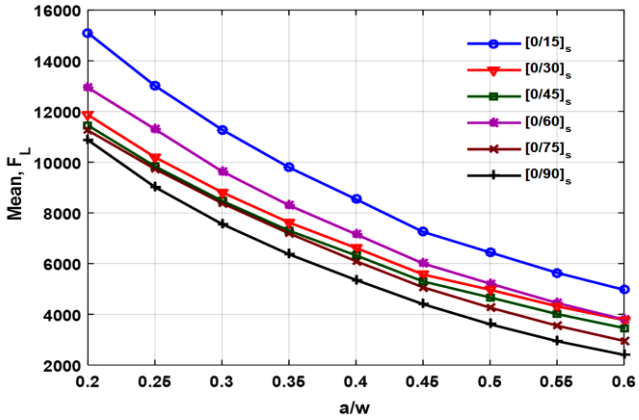

Fig. 4 Effect of the (a/w) ratio on the mean of F_L of $[0/\theta]_s$ LCP

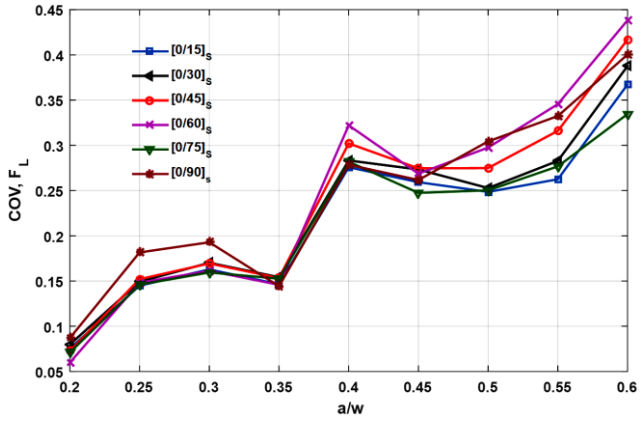

Fig. 5 Effect of the a/w ratio on the COV of F_L of $[0/\theta]_s$ LCP

Table 6 Effect of the inline void on the mean and corresponding COV of F_L of $[0/\theta]_s$ LCP

Stacking sequence $[0/\theta]_s$	L_1=2.5 mm		L_1=3.5 mm		L_1=4.5 mm		L_1=5.5 mm	
	Mean	COV	Mean	COV	Mean	COV	Mean	COV
$[0/15]_s$	4468.9	0.22113	6357.4	0.22394	7301.9	0.23113	7830.4	0.2359
$[0/30]_s$	3535	0.2178	4946.3	0.2286	5668.4	0.23614	6074	0.24215
$[0/45]_s$	3277.5	0.22476	4738.5	0.24524	5426.8	0.25558	5789.9	0.26261
$[0/60]_s$	3528.6	0.22334	5383.1	0.26152	6161.4	0.27493	6546.2	0.28204
$[0/75]_s$	2823.1	0.202562	4839.7	0.27628	5516.4	0.27619	5724.7	0.25986
$[0/90]_s$	2392.7	0.246049	4598.2	0.24952	4939.7	0.25294	5126	0.25616

defined by L_1. L_1 is varied to know the effect of the location of void on the mean and COV of F_L of $[0/\theta]_s$ LCP. The radius (R) of the void is taken as 2 mm, a/w ratio as 0.4 and randomness is considered in crack length 'a' with COC as 0.1. As seen from Table 6, if the void is nearer the crack tip, the mean value of F_L is minimum; this is due to the higher values of stresses at the crack tip due to the interaction effect of the crack tip and void and vice versa if a void is away from the crack tip.

Table 7 Effect of the number of voids on the mean and COV of F_L of $[0/\theta]_s$ LCP

Stacking sequence $[0/\theta]_s$	2 voids		4 voids		Without voids	
	Mean	COV	Mean	Mean	COV	Mean
$[0/15]_s$	6160.2	0.185578	5154.7	0.205704	6442.3	0.24852
$[0/30]_s$	4476.8	0.240772	3680.9	0.24731	4968.4	0.25277
$[0/45]_s$	3924.2	0.238147	3395.6	0.229208	4665.7	0.27491
$[0/60]_s$	3782.7	0.25699	3421.2	0.234599	5211.9	0.29755
$[0/75]_s$	2733.6	0.25684	2625.2	0.24917	4265.1	0.35027
$[0/90]_s$	2474.1	0.29163	2434.8	0.28846	3608.4	0.40435

As the void moves away from the crack tip, the mean of F_L approach the mean of F_L of LCP without any void and COV of the F_L is increasing. $[0/15]_s$ LCP is the best laminate amongst all the $[0/\theta]_s$ LCP because it has maximum mean and minimum COV of F_L which means this laminate is least sensitive to the randomness in crack length and hence more reliable.

To study the effect of the multiple voids on the mean and corresponding COV of F_L of $[0/\theta]_s$ LCP, laminate-4 in Fig. 2(d) is chosen. The results of the mean and corresponding COV of F_L are obtained by choosing two and four numbers of voids adjacent to the crack tip. The location of the void centre from the crack tip is defined by the parameters L_1 and D_1. In this study, L_1 and D_1 lengths are taken as 4mm, the void radius (R) is taken as 3 mm, a/w ratio is 0.5 and randomness is considered in the crack length (a) with COC as 0.1. From Table 7 it is observed that, as the number of voids goes on increasing, the mean of F_L of $[0/\theta]_s$ LCP decreases. This happens because voids in the vicinity of the crack increases SIF at the crack tip due to the interaction effect of void and crack fields. The crack tip stress field is characterized by SIF and hence, increased SIF due to more voids reduces F_L. The presence of more voids also weakens the plate. In the case of $[0/15]_s$ LCP with two and four voids, the mean of F_L is decreased by 4.38% and 19.99% respectively as compared with the mean of FL of $[0/15]_s$ LCP without voids. In the case of $[0/90]_s$ LCP with four voids, the mean of FL is decreased by 32.52% as compared with the mean of F_L of $[0/90]_s$ LCP without the voids. The mean of F_L of $[0/\theta]_s$ LCP is highly affected by the lamination angle (θ) and number of voids. The COV of the F_L of $[0/\theta]_s$ LCP also depends on the lamination angle (θ) and number of voids.

To study the effect of the combined randomness in the input parameters on the mean and corresponding COV of F_L of $[0/\theta]_s$ LCP, laminate-1 in Fig. 2(a) is chosen. For this study, the crack length (a) is taken as 9.5 mm. The different combinations of random variables (RVs) as $b_i[\{i=1, 2\}=0.1]$, $b_i[\{i=1, 2, 5\}=0.1]$ and $b_i[\{i=1, 2, 5, 9\}=0.1]$ are selected for studying the effect of combined randomness in the RVs on the mean and corresponding COV of F_L. As observed from Table 8, as the number of RVs is increased, the COV of F_L of $[0/\theta]_s$ LCP is significantly increasing. If the COVs in different RVs are considered simultaneously, it will cause a compounding effect on the COV of F_L. As more and more sensitive RVs are considered simultaneously, the COV of F_L goes on increasing.

To study the effect of the crack angle (α) on the mean and corresponding COV of F_L of $[0/\theta]_s$ LCP, laminate-2 in Fig. 2(b) is chosen. For this study, the crack length (a) is taken as 9 mm and the combined randomness is considered in the RVs E_1, E_2 and α with COC as 0.1. The crack angle is varied from 10^0 to 30^0. As seen from Table 9, as the crack angle is increased, the mean of F_L of $[0/\theta]_s$ LCP increases and corresponding COV decreases. For $[0/15]_s$ LCP, if the crack angle is varied from 10^0 to 30^0, the mean of F_L increases by 13.22% and the corresponding COV decreases by 30.87%.

Table 8 Effect of the combined randomness in the RVs on the mean and COV of F_L of $[0/\theta]_s$ LCP

Stacking sequence $[0/\theta]_s$	b_i[{i=1, 2 }=0.1]		b_i[{i=1, 2, 5}=0.1]		b_i[{i=1, 2, 5, 9}=0.1]	
	Mean	COV	Mean	Mean	COV	Mean
$[0/15]_s$	5800.5	0.051845	5801	0.61676	5801.2	1.07853
$[0/30]_s$	4463.7	0.056187	4464.1	0.54114	4464.3	1.1146
$[0/45]_s$	4147	0.058973	4147.4	0.69487	4147.6	1.22406
$[0/60]_s$	4581.1	0.065135	4581.6	0.76328	4581.8	1.30918
$[0/75]_s$	3851	0.061932	3851.5	0.75884	3851.7	1.29649
$[0/90]_s$	3250.9	0.067567	3251.3	0.79857	3251.5	1.3464

Table 9 Effect of the crack angle (α) on the mean and corresponding COV of F_L of $[0/\theta]_s$ LCP

Stacking sequence $[0/\theta]_s$	$\alpha=10^0$		$\alpha=20^0$		$\alpha=30^0$	
	Mean	COV	Mean	COV	Mean	COV
$[0/15]_s$	4563.2	0.32425	5009.8	0.306637	5166.3	0.24776
$[0/30]_s$	3156.15	0.3338	3832.8	0.31006	4219.4	0.27163
$[0/45]_s$	3063.19	0.31327	3354.8	0.259014	3875.6	0.23843
$[0/60]_s$	3276.44	0.30287	3403.3	0.250246	3901.1	0.22396
$[0/75]_s$	2584.15	0.37145	2685.5	0.308952	2701.3	0.25286
$[0/90]_s$	2324.4	0.43178	2403.0	0.36059	2588.6	0.30291

Similar observations are seen in the other $[0/\theta]_s$ LCP. Mode I fracture involves the opening of the crack. In the present study, loading considered is a tensile and as the crack angle increases, Mode I fracture severity reduces. Cracks with larger inclinations have increased fracture path length, which demands more energy for crack propagation hence with increase in crack angle F_L increases.

5. Conclusions

In the present study, the statistics of the ultimate failure load of $[0/\theta]_s$ LCP containing the edge crack and voids subjected to the tensile loading are presented. The effect of the different parameters like crack length, number of voids, location of the voids, and crack angle on the mean and corresponding COV of ultimate failure load of $[0/\theta]_s$ LCP is studied. The numerical solution of the ultimate failure load is useful for evaluating the critical SIFs or fracture toughness of the LCP containing cracks and voids by considering the uncertainties in the material properties, geometric parameters, and loading. The important conclusions from this study are as follows,

- $[0/\theta]_s$ LCPs are very sensitive to the randomness in the crack length, applied load, transverse tensile strength of the laminate, and modulus of elasticity of the material, so precise control of these parameters is important for the reliable design.
- As the crack length is increased, the mean of the ultimate failure load decreases and the corresponding COV is increased in all $[0/\theta]_s$ LCP. Minimum and maximum values of the mean of the ultimate failure load are observed in $[0/90]_s$ and $[0/15]_s$ laminates respectively.
- The mean of the failure load is very sensitive if the void is present in line with the crack and

nearer to the crack tip. As the void is moved away from the crack tip mean of the failure load approaches with the mean of the failure load of LCP without a void.

• The mean and corresponding COV of failure load of $[0/\theta]_s$ LCP is greatly influenced by the number of voids and their location. The mean of failure load decreases and corresponding COV increases if the number of voids is increased.

• If the randomness is considered in the number of input system parameters simultaneously, the COV of the failure load increases means the sensitivity of the response is higher.

• As the crack angle is increased from 10^0 to 30^0, the mean of the failure load of $[0/\theta]_s$ LCP increases and the corresponding COV is decreased.

• $[0/15]_s$ LCP is better than the other $[0/\theta]_s$ LCP because it has maximum ultimate failure load and minimum COV hence more reliable. The selection of the lamina orientation is important.

References

Abdullah, N.A., Curiel-Sosa, J.L., Taylor, Z.A., Tafazzolimoghaddam, B., Vicente, J.L.M. and Zhang, C. (2017), "Transversal crack and delamination of laminates using XFEM", *Compos. Struct.*, **173**, 78-85. https://doi.org/10.1016/j.compstruct.2017.04.011.

Asadpoure, A. and Mohammadi, S. (2007), "Developing new enrichment functions for crack simulation in orthotropic media by the extended finite element method", *Int. J. Numer. Method. Eng.*, **69**(10), 2150-2172. https://doi.org/10.1002/nme.1839.

Asadpoure, A., Mohammadi, S. and Vafai, A. (2006), "Crack analysis in orthotropic media using the extended finite element method", *Thin Wall. Struct.*, **44**(9), 1031-1038. https://doi.org/10.1016/j.tws.2006.07.007.

Asadpoure, A., Mohammadi, S. and Vafai, A. (2006), "Modeling crack in orthotropic media using a coupled finite element and partition of unity methods", *Finite Elem. Anal. Des.*, **42**(13), 1165-1175. https://doi.org/10.1016/j.finel.2006.05.001.

Bayesteh, H. and Mohammadi, S. (2013), "XFEM fracture analysis of orthotropic functionally graded materials", *Compos. Part B: Eng.*, **44**(1), 8-25. https://doi:10.1016/j.compositesb.2012.07.055.

Benzaama, A., Mokhtari, M., Benzaama, H., Gouasmi, S. and Tamine, T. (2018), "Using XFEM technique to predict the damage of unidirectional CFRP composite notched under tensile load", *Adv. Aircr. Spacecr. Sci.*, **5**(3), 129-139. https://doi.org/10.12989/aas.2018.5.1.129.

Bhardwaj, G., Singh, I.V. and Mishra, B.K. (2015), "Stochastic fatigue crack growth simulation of interfacial crack in bi-layered FGMs using XIGA", *Comput. Method. Appl. Mech. Eng.*, **284**, 186-229. https://doi.org/10.1016/j.cma.2014.08.015.

Chen, X., Gu, J., Yu, T., Qiu, L. and Bui, T.Q. (2019), "Numerical simulation of arbitrary holes in orthotropic media by an efficient computational method based on adaptive XIGA", *Compos. Struct.*, **229**,111387. https://doi:10.1016/j.compstruct.2019.111387.

Dongen, B.V., Oostrum, A.V. and Zarouchas, D. (2017), "A blended continuum damage and fracture mechanics method for progressive damage analysis of composite structures using XFEM", *Compos. Struct.*, **184**, 512-522. https://doi.org/10.1016/j.compstruct.2017.10.007.

Duarte, A.P.C., Sáez, A.D. and Silvestre N. (2017), "Comparative study between XFEM and Hashin damage criterion applied to failure of composites", *Thin Wall. Struct.*, **115**, 277-288. https://doi.org/10.1016/j.tws.2017.02.020.

Ebrahimi, S.H., Mohammadi, S. and Asadpoure, A. (2008), "An extended finite element (XFEM) approach for crack analysis in composite media", *Int. J. Civil Eng.*, **6**(3), 198-207.

Ezzine, M.C., Amiri, A., Tarfaoui, M. and Madani, K. (2018), "Damage of bonded, riveted and hybrid (bonded/riveted) joints, experimental and numerical study using CZM and XFEM methods", *Adv. Aircr. Spacecr. Sci.*, **5**(5), 129-139. https://doi.org/10.12989/aas.2018.5.5.595.

Gu, J., Yu, T., Van, L., Tanaka, S., Yuan, H. and Bui, T.Q. (2020), "Crack growth adaptive XIGA simulation

in isotropic and orthotropic materials", *Comput. Method. Appl. Mech. Eng.*, **365**, 113016. https://doi.org/10.1016/j.cma.2020.113016.

Haldar, A. and Mahadevan, S. (2000), *Probability, Reliability, and Statistical Methods in Engineering Design*, John Wiley, New York, NY, USA.

Hamdia, K.M., Silani, M., Zhuang, X., He, P. and Rabczuk, T. (2017), "Stochastic analysis of the fracture toughness of polymeric nanoparticle composites using polynomial chaos expansions", *Int. J. Fract. Mech.*, **206**, 215-227. https://doi.org/10.1007/s10704-017-0210-6.

Hulton, A.W. and Cavallaro, P.V. (2016), "Comparing computational and experimental failure of composites using XFEM", *ASME International Mechanical Engineering Congress and Exposition*, Phoenix, AZ, USA, November.

Jiang, S., Du, C., Gu, C. and Chen, X. (2014), "XFEM analysis of the effects of voids, inclusions and other cracks on the dynamic stress intensity factor of a major crack", *Fatig. Fract. Eng. Mater. Struct.*, **37**(8), 866-882. https://doi.org/10.1111/ffe.12150.

Jones, R. (2002), *Mechanics of Composite Material*, McGraw-Hill, New York, NY, USA.

Kaman, O.M. (2011), "Effect of fiber orientation on fracture toughness of laminated composite plates [0/θ]s", *Eng. Fract. Mech.*, **78**(13), 2521-2534. https://doi.org/10.1016/j.engfracmech.2011.06.005.

Khasin, V.L. (2014), "Stochastic model of crack propagation in brittle heterogeneous materials", *Int. J. Eng. Sci.*, **82**, 101-123. https://doi.org/10.1016/j.ijengsci.2014.04.002.

Kim. J.H. and Paulino, G.H. (2002), "Mixed-mode fracture of orthotropic functionally graded materials using finite elements and the modified crack closure method", *Eng. Fract. Mech.*, **69**(14-16), 1557-1586. https://doi.org/10.1016/S0013-7944(02)00057-7.

Lei, J., Wang, Y.W. and Gross, D. (2005), "Analysis of dynamic interaction between an inclusion and a nearby moving crack by BEM", *Eng. Anal. Bound. Elem.*, **29**(8), 802-813. https://doi.org/10.1016/j.enganabound.2005.04.002.

Liu, D., Cao, D., Hu, H., Zhong, Y. and Li, S. (2021), "Numerical study on failure behaviour of open-hole composite laminates based on LaRC criterion and extended finite element method", *J. Mech. Sci. Technol.*, **35**(3), 1037-1047. https://doi.org/10.1007/s12206-021-0217-9.

Lua, Y.J., Liu, W.K. and Belytschko, T. (1993), "Curvilinear fatigue crack reliability analysis by stochastic boundary element method", *Numer. Meth. Eng.*, **36**(22), 3841-3858. https://doi.org/10.1002/nme.1620362206.

Ma, Z., Chen, J., Yang, Q., Li, Z. and Su, X. (2021), "Progressive fracture analysis of the open-hole composite laminates: Experiment and simulation", *Compos. Struct.*, **262**, 113628. https://doi.org/10.1016/j.compstruct.2021.113628.

Martinez, E.R., Chakraborty, S. and Tesfamariam, S. (2021), "Machine learning assisted stochastic-XFEM for stochastic crack propagation and reliability analysis", *Theoret. Appl. Fract. Mech.*, **112**, 102882. https://doi.org/10.1016/j.tafmec.2020.102882.

Mohammadi, S. (2008), *Extended Finite Element Method for Fracture Analysis of Structures*, Blackwell Publishing, Oxford, UK.

Motamedi, D., Milani, A.S., Komeili, M., Bureau, M.N., Thibault, F. and Trudel, B.D. (2014), "A stochastic XFEM model to study delamination in PPS/Glass UD composites: Effect of uncertain fracture properties", *Appl. Compos. Mater.*, **21**, 341-358. https://doi.org/10.1007/s10443-013-9342-7.

Natarajan, S., Kerfriden, P., Mahapatra, D.R. and Bordas, S.P.A. (2014), "Numerical analysis of the inclusion-crack interaction by the extended finite element method", *Int. J. Compos. Method. Eng. Sci. Mech.*, **15**(1), 26-32. https://doi.org/10.1080/15502287.2013.833999.

Nguyen, M.N., Nguyen, N.T., Truong, T.T. and Bui, T.Q. (2019), "Thermal-mechanical crack propagation in orthotropic composite materials by the extended four-node consecutive interpolation element (XCQ4)", *Eng. Fract. Mech.*, **206**, 89-113. https://doi.org/10.1016/j.engfracmech.2018.11.036.

Patel, A., Sato, E., Shichijo, N., Hirata, I. and Takagi, T. (2022), "A mixed XFEM and CZM approach for predicting progressive failure in advanced SiC/SiC CMC component", *Compos. Part C*, **9**, 100325. https://doi.org/10.1016/j.jcomc.2022.100325.

Patil, R.U., Mishra, B.K. and Singh, I.V. (2017), "A new multiscale XFEM for the elastic properties evaluation

of heterogeneous materials", *Int. J. Mech. Sci.*, **122**, 277-287. https://doi.org/10.1016/j.ijmecsci.2017.01.028.

Qin, Q.H. and Lu, M. (2000), "BEM for crack-inclusion problems of plane thermopiezoelectric solids", *Int. J. Numer. Method. Eng.*, **48**, 1071-1088. https://doi.org/10.1002/(SICI)1097-0207(20000710)48:7%3C1071::AID-ME917%3E3.0.CO;2-W.

Sharma, K., Singh, I.V., Mishra, B.K. and Shedbale, A.S. (2013), "The effect of inhomogeneities on an edge crack: A numerical study using XFEM", *Int. J. Compos. Method. Eng. Sci. Mech.*, **14**(6), 505-523. https://doi.org/10.1080/15502287.2013.820227.

Shedbale, A.S., Singh, I.V. and Mishra, B.K. (2013), "Nonlinear simulation of an embedded crack in the presence of holes and inclusions by XFEM", *Proc. Eng.*, **64**, 642-651. https://doi.org/10.1016/j.proeng.2013.09.139.

Shen, X., Hu, H., Wang, Z., Chen, X. and Du, C. (2021), "Stochastic fracture analysis using scaled boundary finite element methods accelerated by proper orthogonal decomposition and radial basis functions", *Geofluids*, **2021**(1), 9181415. https://doi.org/10.1155/2021/9181415.

Singh, I.V., Mishra, B.K., Bhattacharya, S. and Patil, R.U. (2012), "The numerical simulation of fatigue crack growth using extended finite element method", *Int. J. Fatig.*, **36**(1), 109-119. https://doi.org/10.1016/j.ijfatigue.2011.08.010.

Singh, S. and Kumar, A. (1998), "Postbuckling response and failure of symmetric laminates under in-plane shear", *Compos. Sci. Technol.*, **58**(12), 1949-1960. https://doi.org/10.1016/S0266-3538(98)00032-3.

Sukumar, N., Chopp, D.L., Moës, N. and Belytschk, T. (2001), "Modeling holes and inclusions by level sets in the extended finite-element method", *Compos. Method. Appl. Mech. Eng.*, **190**(46-47), 6183-6200. https://doi.org/10.1016/S0045-7825(01)00215-8.

Swati, R.F., Hua, W.L., Elahi, H. and Khan, A.A. (2018), "XFEM damage analysis of carbon fiber reinforced composites and crack propagation in mixed-mode and implementation of the method using ABAQUS", *Int. J. Mater. Mech. Manuf.*, **6**(4), 286-290. https://doi.org/10.18178/ijmmm.2018.6.4.393.

Turan, K., Gur, M. and Kaman, M.O. (2014), "Progressive failure analysis of pin-loaded unidirectional carbon-epoxy laminated composites", *Mech. Adv. Matrt. Struct.*, **21**(2), 98-106. https://doi.org/10.1080/15376494.2012.677109.

Wang, X.F. and Hasebe, N. (2000), "Bending of a thin plate containing a rigid inclusion and a crack", *Eng. Anal. Bound. Elem.*, **24**(2), 145-153. https://doi.org/10.1016/S0955-7997(99)00062-4.

Yu, T. and Bui, T.Q. (2018), "Numerical simulation of 2-D weak and strong discontinuities by a novel approach based on XFEM with local mesh refinement", *Compos. Struct.*, **196**, 112-133. https://doi.org/10.1016/j.compstruc.2017.11.007.

CC